Effect of very high temperature short exposures on the dissolution of the γ′ phase in single crystal MC2 superalloy

Jonathan Cormier · Xavier Milhet · Jose Mendez

Abstract Time-temperature dependence of the γ′ phase volume fraction was investigated for a second generation single crystal nickel-based superalloy exposed to very short high temperature regimes (1,100–1,200 °C). In this temperature range, the dissolution of the strengthening γ′ phase occurs. Evolution of the γ′ volume fraction in transient regimes has been established for each temperature and activation energy of the dissolution phenomenon were determined. They directly attest from the activity of the diffusing species involved during this phenomenon. From these analyses, the volume fraction at equilibrium was established for the entire temperature range where dissolution occurs. A model, based on a time/temperature equivalence, is proposed to quantify the γ′ volume fraction dissolved during short high temperature exposure.

Introduction

Single crystal nickel-based superalloys are mainly used for aeronautic components, more particularly turbine blades. The use of these materials is required because of the range of stresses applied to the turbine blades, going from intermediate temperatures (700–800 °C) and high stresses in the blade root to high temperatures (1,000–1,100 °C) and low stresses in the blade airfoils sections [1]. Single crystal nickel-based superalloys are composed by strengthening γ′ phase precipitates, merged in a γ matrix. Their performance, particularly under creep conditions, depends mainly on the thermal stability of the γ′ phase in the structure [2]. Several studies were carried out in order to identify the role of the volume fraction of the γ′ phase on the creep properties of various superalloys [3, 4]. It was found that the best mechanical resistance is obtained with a γ′ volume fraction $f_{V\gamma'}$ around 70%, higher and lower values leading to a sharp decrease of the creep resistance of the material. From a designer point of view, the enhancement of turboengine efficiency basically requires an increase in the temperature at the entry of the high pressure turbine. The evolution of the morphology of the precipitates (shape, size,...) with or without external loading have been extensively studied or modeled over the past 30 years [5–15]. Generally, these studies where carried out at relatively low temperature and using very long dwell times for materials with lower $f_{V\gamma'}$ values. Very few studies were devoted to determine the evolution of $f_{V\gamma'}$ with the temperature and they generally deal with the material at the thermodynamic equilibrium [16–19]. In these studies, an evolution of the precipitates fraction was found to occur for various superalloys (CMSX4, SRR99, AM1, and MCNG) when heated over 950 °C. It has been shown that the higher the temperature, the more the dissolution phenomenon occurs, while complete dissolution eventually occurs above 1,280 °C. At these temperature levels, the material is subject to great evolutions of its microstructure. This leads to a significant reduction of $f_{V\gamma'}$ and therefore to a loss in mechanical properties.

However, during a flight, turbine blades sometimes experience short high temperature regimes (overheating regimes). On the other hand, machining (drilling holes ...) are known to create localized thermally affected zones. These effects may produce locally a partial dissolution of

J. Cormier (✉) · X. Milhet · J. Mendez
Laboratoire de Mécanique et Physique des Matériaux, UMR CNRS 6617, ENSMA, BP 40109, Futuroscope Chasseneuil Cedex, Poitiers 86961, France
e-mail: jonathan.cormier@lmpm.ensma.fr

the γ' phase and probably reduce subsequently the creep resistance of the material. Little experimental work was performed on the dissolution reaction $\gamma' + \gamma \rightarrow \gamma$ at very high temperature during transient regimes (short exposures at high temperature compared to the time needed to reach the thermodynamic equilibrium) [14, 18, 20]. In this case, to the authors' knowledge, the experimental conditions were far from conditions encountered by the material in service since the heating rates were generally too low to account for a pure high temperature effect. The knowledge of the kinetics of dissolution during transient regimes is an important issue for a better understanding of the in-service behavior of the material. This paper focuses on the evolution of the amount of γ' phase during transient regimes exposed to very high temperatures (1,100, 1,150, and 1,200 °C) and very short times. A special attention was paid to the heating and cooling rates.

Material and experimental techniques

MC2 is a second generation superalloy designed by ON-ERA for single crystalline high pressure turbine blades of helicopter turboshaft engines [21]. The microstructure of this material consists of cubical strengthening precipitates (average edge length $\approx$0.4 μm) of L_{12} γ' phase (Ni₃Al type) merged in a fcc γ matrix [22] (see Fig. 1). The composition in weight percent of MC2 is given in Table 1. After solution heat treatment, aging was performed on the specimens using the following procedure: 6 h at 1,080 °C—air quenched –20 h at 870 °C—air quenched to obtain $f_{V\gamma'}$ around 70%.

The γ' dissolution was studied in isothermal conditions for different dwell times. For this purpose, short exposures at high temperature were performed using a radiant furnace since this set-up is able to reach fast heating and cooling rates. A specific procedure was developed in order to
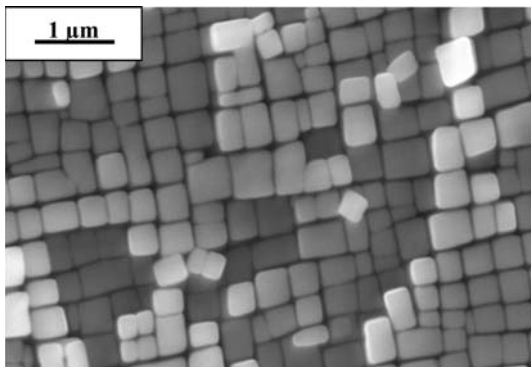
Fig. 1 As-received MC2. The microstructure, obtained after thermal treatment, is built with 70% of γ' coherent cubic precipitates merged within a γ matrix

Table 1 Weight composition of the MC2 single crystal superalloy (in wt.%)

Ni	Cr	Co	Mo	W	Al	Ti	Ta
Bal.	8	5	2	8	5	1.5	6

prevent any artifacts arising from dissolution during the heating/cooling ramp. This procedure consists in a jump from room temperature up to 700 °C at 17 °C s^{-1} followed by a ramp from 700 °C to the target temperature at 1 °C s^{-1}. After a dwell time at this temperature, the material was quenched (cooling rate 10 °C s^{-1} approximately) to prevent the microstructure from evolving greatly during this step.

Some other tests where performed using a resistive furnace and using a special rig. While the former allows slow heating and cooling rates, the latter can achieve heating and cooling rate higher than 50 °C s^{-1}.

The dissolution tests were performed on small cylinders (10 mm diameter, 10 mm height) cut from single-crystalline rods with an axis within 5° from the crystallographic direction [001].

Observations of the microstructure after high temperature exposures were performed using a Scanning Electron Microscope (SEM) JEOL 6400 operating at 20 kV. After each heat treatment, 30 μm were ground from the surface of the specimen to remove the oxide layer developed during aging time at maximum temperature. Selective etching of the γ phase was used to observe the microstructure. This chemical etching proved to be particularly helpful to obtain a better contrast between the two phases. In addition, this technique allows more accurate measurements of the surface fraction $f_{S\gamma'}$ of γ' phase since no precipitates are etched away. Images were recorded at an appropriate magnification to observe a large amount of γ' precipitates. For each specimen, the γ' surface fraction $f_{S\gamma'}$ was determined by image analysis. Each image was recorded and processed using the same routine: (1) after smoothing the contour, the contrast is enhanced; (2) the black and white image is eroded after brightness thresholding has been performed, then reconstructed in order to eliminate all the particles that are not representative of the microstructure at high temperature; (3) the surface fraction $f_{S\gamma'}$ of the precipitates is quantified. A minimum of 7 observations is used for each heat treatment to give an accurate estimation of $f_{S\gamma'}$. No distinction will be made between the γ' quantification carried out either in the dendritic or in the interdendritic areas of the material since difference is within uncertainty of the results ($\pm$3% on the surface fractions). Since the γ' precipitates remains close to a cubic shape, the volume fraction $f_{v\gamma'}$ can be directly determined by $f_{S\gamma'} = f_{S\gamma'}^{3/2}$ [16].

## Results and discussion

γ′ volume fraction

Samples were held at 1,100, 1,150, and 1,200 °C for a time range varying from 5 to 45 min. Microstructures obtained after different short dwell times at 1,200 °C are presented in Fig. 2. At such temperatures, the dissolution of the γ′ strengthening phase starts rapidly (Fig. 2a): precipitates start to dissolve at their corners. Whatever the specimen, as seen on Fig. 2b and c, a fine precipitation is observed in the γ-channels. These ultrafine particles are known to appear from the supersaturated matrix during cooling to room temperature [1, 23–25]. According to previous work, they can only be avoided if the cooling rate is faster than 170 °C s^{-1} [15]. They arise from the dissolved fraction of the initial precipitates and should be erased during the image analysis since they are not characteristic from the microstructure at high temperature.

From Fig. 2, it is clear that the fraction of the γ′ phase decreases rapidly (after less than 30 min). The γ′ cubic precipitates do not dissolve homogeneously. Some zones are free of precipitates (arrows Fig. 2c) while others are close to the as-received microstructure, only slightly reduced in size.

The surface fraction values $f_{S\gamma'}$ obtained for various dwell times at 1,100, 1,150, and 1,200 °C are presented in Fig. 3. Figure 3 plots the evolution of $f_{S\gamma'}$ for the three different temperatures against dwell time, starting from an initial measured value of 73%. The same trend is observed for the three temperatures mentioned above but slightly delayed in time since diffusion kinetics depends on the temperature. As expected, the higher the temperature, the faster the dissolution rate, and for a given temperature, a longer dwell time leads to a lower γ′ surface fraction after high temperature exposure. In this study, $f_{S\gamma'}$ never reached an asymptote, even after a 45-min exposure at any of the three temperatures. Therefore, the material is not yet at thermodynamic equilibrium and $f_{v\gamma'}$ is still in a transient regime. This is in agreement with previous studies showing that the equilibrium volume fraction is obtained after at least 70 min at 1,240 °C for the single crystal Ni-based super alloy AM1 [14] and after 12 h at 1,140 °C in the case
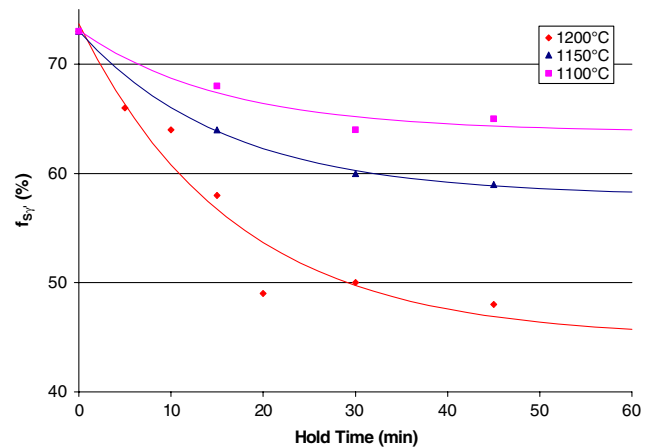
Fig. 3 Evolution of the surface fraction with the time spent under high temperature regime without load. Plotted curves result from Eq. (1)

of Udimet 720 [20]. Assuming an equilibrium volume fraction for an infinite dwell time, the transient regime of the dissolution for a given temperature can be modeled by an asymptotic decreasing exponential law:

$$f_{S\gamma'} = f_{S\,lim} + f_1 \exp\left(\frac{-t}{t_1}\right) \tag{1}$$

where t_1 is the characteristic time for dissolution, f_1 a constant depending on the temperature and $f_{S\,lim}$, the γ′ surface fraction at thermodynamic equilibrium. The parameters t_1 and f_1 deduced from the experimental results are reported in Table 2.

The value of $f_{S\,lim}$, derive from Eq. (1) for each temperature: $f_{S\,lim} = 51.0\%$ at 1,100 °C, 44.1% at 1,150 °C and 30.1% at 1,200 °C. These values are comparable to experimental data (see Table 3) obtained by image analysis

Table 2 Parameters for $f_{S\gamma'}$ modeling

T (°C)	$f_{S\,lim}$ (%)	f_1 (%)	t_1 (min)
1100	63.8	9.3	15.7
1150	57.9	15.1	16.0
1200	44.9	28.8	16.8

Fig. 2 Microstructures after different aging at 1,200 °C: (**a**) 5 min: initial location of the dissolution is at the precipitate angles; (**b**) 30 min; (**c**) 45 min: arrows indicate that the dissolution is inhomogeneous
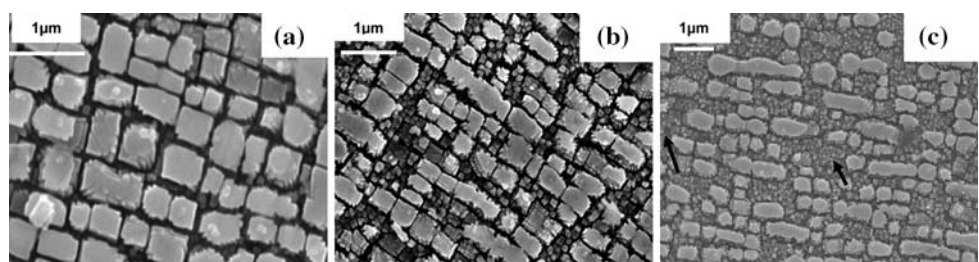
Table 3 $f_{V\gamma'}$ at thermodynamic equilibrium (average uncertainty = 2%)

Temperature (°C)	$f_{V\gamma'}$ (%) measured	$f_{V\gamma'}$ (%) calculated
1100	53.7	51
1150	43.1	44.1
1200	31.2	30.1

from specimens heat treated until thermodynamic equilibrium at ONERA.

Dissolution kinetics

The knowledge of $f_{V\gamma'}$ at any time of the heat treatment is probably not the only important parameter for the material. Since it can be subjected to short exposures at very high temperature during in-service conditions, dissolution kinetics may also be an essential feature: long times at low temperatures may be less harmful than shorter times at very high temperature. The dissolution kinetics was estimated using the experimental results obtained for the three temperatures. Since the dissolution is diffusion-controlled, it is assumed that its kinetics k can be simply described by a Boltzmann law:

$$k = A \exp\left(\frac{-Q}{RT_K}\right) \tag{2}$$

with Q, the apparent activation energy for the diffusion process, T_K the absolute temperature and R the universal gas constant ($R = 8.314$ J K^{-1} mol^{-1}). Starting from the parameters identified using Eq. (1), the kinetics of dissolution, for each temperature can be expressed by:

$$k_{|t} = \frac{\mathrm{d}f_{S\gamma'}}{\mathrm{d}t}_{|t} = -\frac{f_1}{t_1}\exp\left(\frac{-t}{t_1}\right). \tag{3}$$

The results are given in table 4 for different values of dwell time. Comparing the kinetics at 1,100, 1,150, and 1,200 °C, it is noticed that their value doubles when the temperature increases by 50 °C. In this domain, a slight increase in temperature significantly affects the stability of the γ' phase, likely to cause a drastic loss of mechanical properties because of the drop in structural hardening. The apparent activation energies of the dissolution, indicating the diffusion of atomic species, are listed in Table 4. Q increases with t, starting form 180 kJ mol^{-1}, at the beginning of the reaction, up to 200 kJ mol^{-1} after 30 min. The time dependence of the activation energy can result from the fact that when t increases, the volume fraction of γ' involved during the dissolution process decreases until steady-state at equilibrium. When the material is far from equilibrium, the dominant phenomenon is dissolution of

Table 4 Dissolution kinetics and apparent activation energies of the dissolution under various temperature and reaction progress

Dwell time(min)	Temperature (°C)	Kinetics (k min^{-1})	Q (kJ mol^{-1})
0	1,100	-5.9×10^{-3}	179
	1,150	-9.4×10^{-3}	
	1,200	-1.71×10^{-2}	
15	1,100	-2.30×10^{-3}	187
	1,150	-3.7×10^{-3}	
	1,200	-7×10^{-3}	
30	1,100	-8.8×10^{-4}	196
	1,150	-1.45×10^{-3}	
	1,200	-2.9×10^{-3}	

the γ', which should be easy at the very beginning of the thermal exposure. Indeed, when the reaction progresses towards thermodynamic equilibrium, $f_{V\gamma'}$ reaches an asymptotic value $f_{V\ lim}$ corresponding to a stable microstructure, which slows down the dissolution. Compared to the activation energies determined in a previous study by means of tracer elements [26] (285 kJ mol^{-1} for autodiffusion of Ni), 249 kJ mol^{-1} for diffusion of Al in Ni, the low apparent activation energy Q measured in this study may arise from complex events possibly involved during high temperature transient regimes (diffusion heterogeneities linked with the dendritic structure of the material, cooperative diffusion of more than one element...). Furthermore, it is known from the literature that the variation of the concentration C of γ' forming elements with temperature could slightly modify the activation energy since the pseudo-binary diagram does not consist of straight vertical lines in the relevant temperature range [20]. From our experiments; an average value of $Q = 190$ kJ mol^{-1} is chosen for the characterization of the γ' phase dissolution during the transient regime.

Application: quantification of the dissolution under very short overheating regimes

Very short and abrupt overheating regimes between 1,050 and 1,200 °C can occur during in-flight emergency conditions. In this case, the temperature changes rapidly within seconds and the material can be exposed to very high temperature up to several seconds. Three sets of experiments have been carried out using various heating and cooling rates. Different short dwell times were applied to the material at 1,200 °C. A quantification of the dissolved surface fraction was performed (Table 5). It is clear that the thermal history, in terms of heating and cooling rates, greatly influence the material residual microstructure especially for the same time spent at 1,200 °C.

Table 5 Comparison between measured and calculated $f_{S\ diss}$ for various conditions of dwell time, dwell time temperature T_m, heating and cooling rates

Dwell time (min)	T_m (°C)	Heating rate (°C s^{-1})	Cooling rate (°C s^{-1})	t_{equ} (min)	Measured $f_{S\ diss}$ (%)	Calculated $f_{S\ diss}$ (%)
20	1,100	0.4	0.5	26.9	7.4	7.6
20	1,150	0.4	0.5	27.4	11.2	12.4
5	1,200	0.2	0.4	19.2	8.7	19.6

In the following part, an evaluation of the effect of the heating/cooling rates on the dissolution of the γ'-phase is proposed. Experimentally, short overheating can be viewed as trapezoidal cycles. To simplify matters, a time–temperature equivalence is sought to replace this cycle: the trapezoidal cycle with dwell time at T_m, and with heating and cooling rates $\dot{T}_h$ and $\dot{T}_c$ is replaced by a rectangular cycle of equivalent hold time t_{equ} at maximum temperature T_m (Fig. 4).

In this context, t_{equ} is the sum of three terms: $t_{equ,h}$ and $t_{equ,c}$ the equivalent times for the heating and cooling ramps respectively and t_m for the aging at the maximum temperature T_m. For diffusion controlled phenomena, the heating ramp from T_i to T_m can be assimilated to a hold time $t_{equ,h}$ [18]:

$$t_{equ,h} = \int_{t_i}^{t_f} \exp\left[-\frac{Q}{R}\left(\frac{1}{T} - \frac{1}{T_m}\right)\right] dt \quad (8)$$

where Q is the activation energy for the dissolution of the γ'-phase, t_i and t_f, respectively the time at the beginning and the end of the ramp. The term $\frac{1}{T}$ can be replaced by an equivalent expression $\frac{1}{\dot{T}_h(t-t_f)+T_m}$ representing the heating ramp before T_m. The Eq. (8) becomes:

$$t_{equ,h} = \int_{t_i}^{t_f} \exp\left[-\frac{Q}{R}\left(\frac{1}{\dot{T}_h(t-t_f)+T_m} - \frac{1}{T_m}\right)\right] dt \quad (9)$$

Based on the assumption that the time spent at high temperature is much longer than the time needed to reach the temperature plateau, we have $\left|\frac{\dot{T}_h(t-t_f)}{T_m}\right| = \left|\frac{T-T_m}{T_m}\right|$ and

$\left|\frac{T-T_m}{T_m}\right| \prec\prec 1$. when the dissolution is in progress, Eq. (9) can be simplified:

$$t_{equ,h} \approx \int_{t_i}^{t_f} \exp\left(\frac{Q\dot{T}_h(t-t_f)}{RT_m^2}\right) dt \quad (10)$$

after integration, $t_{equ,h}$ can be reduced to the simple relation:

$$t_{equ,h} \approx \frac{RT_m^2}{Q\dot{T}_h} \quad (11)$$

The same approach can be taken for the cooling ramp and the equivalent time t_{equ} at T_m for the entire cycle is the sum of the two $t_{equ,h} + t_{equ,c}$ leading to the following expression:

$$t_{equ} = \frac{T_m^2 R}{Q}\left(\frac{1}{\dot{T}_h} + \frac{1}{\dot{T}_c}\right) + t_m \quad (12)$$

The introduction of the equivalent time t_{equ} in Eq. 1 for a given temperature allows an estimation of the dissolved volume fraction $f_{V\ diss}$ of precipitates for various non-iso-thermal conditions in the temperature regimes where the dissolution reaction $\gamma' + \gamma \rightarrow \gamma$ is effective. It was chosen to calculate $f_{V\ diss}$ instead of the remaining volume fraction since the initial volume fraction of the material could slightly evolve from the optimal value of 70%, depending on both the chemistry of the material and the initial thermal treatment. A good agreement between calculations and experimental measurements is observed for two non-iso-thermal conditions [heating at 0.4 °C s^{-1} + 20 min at 1,100 °C + cooling at 0.5 °C s^{-1} and heating at 0.4 °C + 20 min at 1,150 °C + cooling at 0.5 °C s^{-1}], whereas a great departure is obtained for other conditions [heating at 0.2 °C s^{-1} + 5 min at 1,200 °C + cooling at 0.4 °C s^{-1}] (Table 5). The difference between the calculation and the experiment may arise, in this particular case, from the hypothesis $\left|\frac{T-T_m}{T_m}\right| \prec\prec 1$ which is not verified since the heating and cooling ramps are long compared to the time spent at high temperature. It can be estimated,

Fig. 4 Time–temperature equivalence for replacing a thermal cycle by an aging time t_{equ} at the equivalent temperature T_m
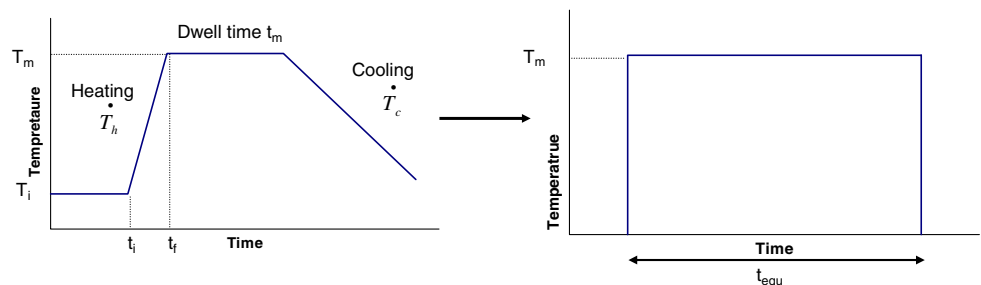
from our experimental results on MC2, that the model is only valid for heating and cooling rates higher than 0.3 °C s^{-1} and when the dwell time at T_m is long enough in comparison with the ramp duration. Some examples of dissolved volume fraction $f_{V\,diss}$ for various conditions and experimental set-up are presented in Table 6. Numerical values of heating and cooling rates presented in Table 6 are the highest ones that can be achieved by the experimental set-ups with an adequate control of the temperature. When comparing the dissolved volume fractions f_{diss}, it appears that the radiant furnace ($\dot{T}_h = \dot{T}_c = 5\,°C\,s^{-1}$) and the special equipment ($\dot{T}_h = \dot{T}_c = 60\,°C\,s^{-1}$) achieved very close microstructures, contrary to the results obtained with the resistive furnace ($\dot{T}_h = \dot{T}_c = 0.4\,°C\,s^{-1}$), especially when dwell times are short. The three different experiments tend to produce the same microstructure for dwell times over 20 min at 1,200 °C, e.g. when the material tends to the thermodynamic equilibrium. These results underline the significant impact of heating and cooling rates on $f_{V\,diss}$ in the case of experiments dedicated to the simulation of short very high temperature overheating regimes which may greatly affect the creep resistance of the material. These are not so important when testing the material over long time under high temperature exposure. From the results shown in this paper, it can be concluded that the model works best when the heating and cooling durations are negligible compared to dwell times at T_m. It can work for all thermal cycles within this limitation. This can be summed up as follows. If the dwell time t_m at the maximum temperature T_m is shorter than 5 min, the material is far from the thermodynamic equilibrium. In this case, $\dot{T}_h$

and $\dot{T}_c$ both should be no less than 1.7 °C s^{-1} approximately so that the time spent to heat up the material t_{heat} (or the time to cool it down after the overheating stage t_{cool}) represents less than $5.t_m$. On the other hand, if the dwell time t_m at T_m lasts over 20 min, the material is close to thermodynamic equilibrium. In this case, the time spent to heat up the material t_{heat} (or the time to cool is down after the overheating stage t_{cool}) amounts to less than $2.5.t_m$, which can easily be performed by any furnace.

In all the experimental results presented in this paper, the material was only exposed to brief very high temperature plateau. Applying a mechanical stress to the material in these conditions would probably modify the microstructures shown here, particularly because the γ' rafting may start.

Conclusions

The following conclusions can be drawn from this study:

(1) The γ' phase dissolution in nickel-based superalloy is strongly dependent on the thermal history of the material. Parameters such as the temperature, the dwell time under high temperature and heating/cooling rates greatly influence the amount of dissolved precipitates in the temperature range where the phenomenon occurs.

(2) The apparent activation energy for dissolution during the transient regime is lower than the one reported in the literature for Ni autodiffusion or Al diffusion in Ni. This can be attributed to more complex phenomena than single element diffusion in a pure solid solution.

(3) The use of a transient modeling of the dissolution allows an accurate determination of the evolution of the thermodynamic equilibrium volume fractions with temperature, without testing the material until these conditions. The prediction of $f_{V\gamma'}$ at thermodynamic equilibrium is of great interest when comparing the creep response of the superalloys at very high temperature, when dissolution occurs.

(4) Using the apparent activation energy, the dissolved volume fraction during non-isothermal conditions was calculated. These calculations may be very useful to understand the mechanical behavior of the superalloys for a given time/temperature loading, especially in case of short overheatings.

Table 6 Examples of dissolved volume fraction $f_{V\,diss}$ for trapezoid cycles where the maximum temperature is 1,200 °C. The activation energy used is 190 kJ mol^{-1}

Dwell time at 1,200 °C (min)	Heating rate (°C s^{-1})	Cooling rate (°C s^{-1})	t_{equ} (min)	$f_{V\,diss}$ (%)
0.5	60	60	0.6	0.3
	5	5	1.1	1.5
	0.4	0.4	10	15
2.5	60	60	2.6	4.3
	5	5	3.1	5.3
	0.4	0.4	12	17
5	60	60	5.1	8.5
	5	5	5.6	9.4
	0.4	0.4	14.5	19.3
20	60	60	20.1	23.1
	5	5	20.6	23.4
	0.4	0.4	29.5	27.1

Heating and cooling rates introduced represent, for increasing values, a resistance furnace, a radiant furnace and a special device developed in the laboratory

References

1. Erickson GL (1996) In: Kissinger RD, Deye DJ, Anton DL, Cetel AD, Nathal MV, Pollock TM, Woodford DA (TMS) (eds) Superalloys 1996. Warrendale, p 35
2. Royer A, Bastie P, Veron M, (1999) Scr Mater 40:955
3. Caron P (1995) Colloque National Superalliage Monocristallin. Toulouse
4. Murakumo T, Kobayashi T, Koizumi Y, Harada H (2004) Acta Mater 52:3737
5. Ardell AJ, Nicholson RB (1966) Acta Metallur 14:1295
6. Tien JK, Copley SM (1971) Met Trans 2:215
7. Svoboda J, Lukas P (1996) Acta Mater 44:2557
8. Louchet F, Hazotte A (1997) Scr Mater 37:589
9. Prikhodko SV, Ardell AJ (2003) Acta Mater 51:5001
10. Prikhodko SV, Ardell AJ (2003) Acta Mater 51:5013
11. Prikhodko SV, Ardell AJ (2003) Acta Mater 51:5021
12. Pollock TM, Argon AS (1994) Acta Metallur Mater 42:1859
13. Pollock TM, Field R, Murphy W (1998). In: Science ICO (ed) Modelling of microstructural evolution in creep resistant materials. Center for continuing education, London, p 193
14. Grosdidier T, Hazotte A, Simon A. (1998) Mater Sci Eng A 256:183
15. Grosdidier T, Hazotte A, Simon A (1994) Scr Metallur Mater 30:1257
16. Diologent F (2002) PhD thesis, Université de Paris Sud—Centre d'Orsay
17. Serin K, Gobenli G, Eggeler G (2004) Mater Sci Eng A 387–389:133
18. Soucail M, Bienvenu Y (1996) Mater Sci Eng A 220:215
19. Roebuck B, Cox D, Reed R (2001) Scr Mater 44:917
20. Monajati H, Jahazi M, Bahrami M, Yue S (2004) Mater Sci Eng A 373:286
21. Fournier D (1995) Colloque National Superalliage Monocristallin. Toulouse
22. Benyoucef M, Coujou A, Barbker B, Clement N, (1997) Mater Sci Eng A 234–236:692
23. Kakehi K (1999) Metallur Mater Trans 30A:1249
24. Brass AM, Roux D, Chene J (2002) Mater Sci Eng A 323:97
25. Duval S, Chamberland S, Caron P, Blavette D, (1994) Acta Metallur Mater 42:185
26. Weast RC (ed) (1985) Handbook of chemistry and physics, 66th edn. CRC Press